Collapse of Landau Levels in Gated Graphene Structures

Nan Gu, Mark Rudner, Andrea Young, Philip Kim, and Leonid Levitov

Phys. Rev. Lett. **106**, 066601 — Published 9 February 2011

DOI: 10.1103/PhysRevLett.106.066601

Landau Level Collapse in Gated Graphene Structures

Nan Gu,[1] Mark Rudner,[2] Andrea Young,[3] Philip Kim,[3] and Leonid Levitov[1]

[1]*Department of Physics, Massachusetts Institute of Technology, 77 Massachusetts Ave, Cambridge, MA 02139*
[2]*Department of Physics, Harvard University, 17 Oxford St., Cambridge, MA 02138*
[3]*Department of Physics, Columbia University, New York, NY10027*

We describe a new regime of magnetotransport in two dimensional electron systems in the presence of a narrow potential barrier. In such systems, the Landau level states, which are confined to the barrier region in strong magnetic fields, undergo a deconfinement transition as the field is lowered. Transport measurements on a top-gated graphene device are presented. Shubnikov-de Haas (SdH) oscillations, observed in the unipolar regime, are found to abruptly disappear when the strength of the magnetic field is reduced below a certain critical value. This behavior is explained by a semiclassical analysis of the transformation of closed cyclotron orbits into open, deconfined trajectories. Comparison to SdH-type resonances in the local density of states is presented.

Electron cyclotron motion constrained by crystal boundaries displays interesting phenomena, such as skipping orbits and electron focusing, which yield a wealth of information on scattering mechanisms in solids [1, 2]. Since the 1980s, semiconducting two-dimensional electron systems (2DES) have become a vehicle for investgating the interplay between gate-induced potential and cyclotron motion. A variety of interesting phenomena were explored in these systems, including quenching of the quantum Hall effect [3, 4], Weiss oscillations due to commensurability between cyclotron orbits and a periodic grating [5], pinball-like dynamics in 2D arrays of scatterers [6], and coherent electron focusing [7].

The experimental realization of graphene [8], a new high-mobility electron system, affords new opportunities to explore effects that were previously inaccessible. Here we focus on one such phenomenon, the transformation of the discrete Landau level spectrum to a continuum of extended states in the presence of a static electric field. Previous attempts to induce sharp potential barriers in III-V semiconductor structures have been limited by the depth at which the 2DES is buried—typically about 100 nm below the surface[9]. In contrast, electronic states in graphene, a truly two-dimensional material, are fully exposed and thus allow for potential modulation on $\sim 10\,\mathrm{nm}$ length scales using small local gates and thin dielectric layers[10–13].

To probe the phenomena of interest, barrier widths must be comparable to the magnetic length $\ell_B = (\hbar c/eB)^{1/2}$ for the fields in which magnetic oscillations can be observed. This condition gives characteristic fields as low as 30 mT for systems such as GaAs. Magnetic oscillations are nearly washed out at such fields, making the effects described below hard to probe in GaAs structures. In contrast, the gate widths available in graphene translate to much higher fields of a few Tesla, making graphene the system of choice for this experiment.

The behavior which will be of interest for us is illustrated by a toy model involving the Landau levels of a massive charged particle in the presence of an inverted parabolic potential $U(x) = -ax^2$. Competition between the repulsive potential and magnetic confinement gives rise to a modified harmonic oscillator spectrum

$$\varepsilon_n(p_y) = \frac{\hbar e}{m}\sqrt{B^2 - B_c^2}\,(n + 1/2) - \frac{2ap_y^2}{e^2(B^2 - B_c^2)} \quad (1)$$

for $B > B_c$, where m is the particle mass, p_y is the y component of momentum, and $B_c = \sqrt{2ma}/e$ is the critical magnetic field strength. For strong magnetic field, $B > B_c$, the spectrum consists of discrete (but dispersive) energy bands indexed by an integer n, whereas for $B \le B_c$ the spectrum is continuous even for fixed p_y. This behavior can be understood quasiclassically in terms of transformation of closed cyclotron orbits into open orbits, which occurs when the Lorentz force is overwhelmed by the repulsive barrier potential.

Landau levels of massless Dirac charge carriers in single-layer graphene, subject to a linear potential $U(x) = -eEx$, exhibit an analogous collapse of the discrete spectrum [15]:

$$\varepsilon_n(p_y) = \pm v_F\sqrt{2n\hbar eB}\left(1 - \beta^2\right)^{3/4} - \beta v_F p_y, \quad (2)$$

where $n = 0, 1, 2...$ and $\beta = E/v_F B$. The transition at $B_c = E/v_F$ can be linked to the classical dynamics of a massless particle, characterized by closed orbits at $B > B_c$ and open trajectories at $B < B_c$ [16].

A simple picture of the spectrum (2) can be obtained from the Bohr-Sommerfeld (BS) quantization condition

$$\int_{x_1}^{x_2} p_x(x)dx = \pi\hbar(n + \gamma), \quad (3)$$

where x_1 and x_2 are the turning points, $\gamma = 0$ due to the Berry phase contribution for Dirac fermions, and

$$p_x(x) = \sqrt{(\varepsilon - U(x))^2/v_F^2 - (p_y - eBx)^2}. \quad (4)$$

For linear $U(x)$, this gives the Landau level spectrum (2) for $B > B_c$. As B approaches B_c, one of the turning points moves to infinity, indicating a transformation of closed orbits into open trajectories.

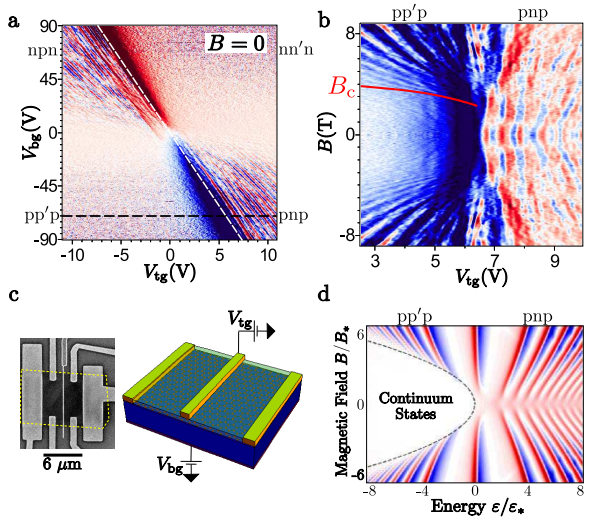

FIG. 1: (a) Differentiated conductance, $dG/dV_{\rm tg}$, of a narrow top gate graphene device, pictured in (c). Fabry-Perot (FP) oscillations appear in the presence of confining pn junctions. (b) $dG/dV_{\rm tg}$ as a function of B and $V_{\rm tg}$. Shubnikov-de Haas (SdH) oscillations are observed at high B. The fan-like SdH pattern is altered by the barrier: in the pp′p region it curves, weakens, and is washed out at fields $|B| \lesssim B_c$, Eq.(7), while in the pnp region a crossover to FP oscillations occurs. Data shown correspond to $V_{\rm bg} = -70$V [dashed line in (a)]. (c) Top gated graphene device micrograph and schematic; top gate width is $\sim$ 16nm. (d) Local density of states (DOS) in the middle of parabolic barrier. The energy derivative $dN/d\varepsilon$ [see Eq.(10)], which corresponds to the measured quantity $dG/dV_{\rm tg}$, is shown. Dashed parabola marks the critical field, Eq.(8). Oscillations in the DOS modulate the rate of scattering by disorder, resulting in the SdH effect [18].

To realize the collapse of Landau levels in an electron system, several conditions must be met. First, it must be possible to create a potential barrier that is steep on the scale of the cyclotron orbit radius. Second, the system must be ballistic on this length scale, in order to suppress the broadening of Landau levels due to disorder. Graphene, which is a truly two-dimensional material with high electron mobility, fulfills both conditions. Crucially, as demonstrated by the recent observation of Fabry-Perot (FP) oscillations in gated graphene structures [13], transport can remain ballistic even in the presence of a gate-induced barrier. Thus graphene is an ideal system for studying the Landau level collapse.

Transport data taken from a locally gated device similar to that described in Ref.[13] are shown in Fig.1. Graphene was prepared via mechanical exfoliation and contacted using electron beam lithography before being coated with a 7/10 nm thick hydrogen silsesquioxane/HfO_2 dielectric layer. Narrow ($\sim$16 nm) palladium top gates were then deposited, and the electrical resistance measured at 1.6 Kelvin. Finite element modeling[13] yields density profile

$$e\rho(x) \approx \frac{C_{\rm tg}V_{\rm tg}}{1+x^2/w^2} + C_{\rm bg}V_{\rm bg}, \qquad (5)$$

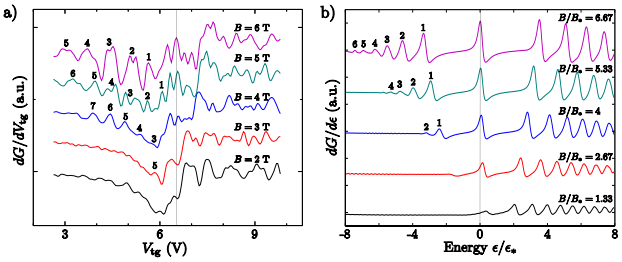

FIG. 2: (a) Traces of the conductance data from Fig.1b for several magnetic field values. Landau level numbers are shown next to the corresponding peaks. The SdH oscillations abruptly disappear in the unipolar (pp′p) region as the magnetic field is lowered to $B \approx 3$ T, and yet persist to much lower fields in the pnp region. (b) Traces of the calculated local DOS (see Fig.1d) showing similar behavior. The traces are artificially offset from each other for visual clarity. In both plots, as the magnetic field is lowered, higher number Landau Levels collapse first, indicating a dependence of the critical field B_c on energy/gate voltage.

with $w \approx 45$ nm, where $C_{\rm tg(bg)}$ and $V_{\rm tg(bg)}$ are the top (bottom) gate capacitance and applied voltage. To subtract the series resistances of the graphene leads, the numerical derivative of the conductance with respect to the top gate voltage, $dG/dV_{\rm tg}$, was analyzed.

At zero magnetic field (Fig.1a), $dG/dV_{\rm tg}$ shows distinct behavior in four regions in the ($V_{\rm bg}$, $V_{\rm tg}$) plane, corresponding to pp′p, pnp, npn, and nn′n doping, where n (p) refers to negative (positive) charge density and prime indicates different density. The appearance of FP interference fringes when the polarity of charge carriers in the locally gated region and graphene leads have opposite signs indicates that the mean free path is comparable to the barrier width, $l_{\rm mf} \sim w$.

In high magnetic field, a fan of SdH resonances corresponding to Landau levels is seen in both the bipolar and unipolar regimes (see Fig.1b). At lower fields, the observed behavior depends on the polarity under the gate. In the bipolar regime, as B is lowered, the SdH resonances smoothly evolve into FP resonances. The half-period shift, clearly visible in the data at $B \approx 1$ T, is a hallmark of Klein scattering [14]. In the unipolar regime, the SdH resonances bend, becoming more horizontal at lower field. The oscillations first begin to lose contrast, and then completely disappear below $B_c \approx 4$ T (Fig.2).

The connection between this behavior and Landau level collapse is exhibited most clearly by a semiclassical analysis. The SdH resonances arise from an oscillatory contribution to the density of states at the Fermi level due to closed trajectories; the BS condition (3) with $\varepsilon = \varepsilon_F$ and $p_y = 0$ gives a good estimate for the positions of those resonances. For a generic barrier potential, Eq.(3) can be written directly in terms of experimental control parameters. Using the Thomas-Fermi approximation, and ignoring the effects of 'quantum capacitance' and nonlinear screening [17], we define the position-dependent Fermi momentum $k_F(x) = \sqrt{4\pi\rho(x)/g}$, where $g = 4$

is the spin/valley degeneracy. Substituting the relation $\varepsilon - U(x) = \hbar v_F k_F(x)$ into Eq.(4), we obtain

$$\int_{x_1}^{x_2} \sqrt{\frac{4\pi}{g}\hbar^2\rho(x) - (p_y - eBx)^2}dx = \pi\hbar(n+\gamma). \quad (6)$$

Interestingly, and somewhat unexpectedly, the quantization condition assumes the same form for massless and massive carriers with $g = 4$ (monolayer and bilayer graphene); it would thus be trivially modified for GaAs quantum wells ($g = 2$ and $\gamma = 1/2$).

A rough estimate for the critical field can be obtained by comparing the curvature of $\rho(x)$ at $x = 0$ with the B^2x^2 term in Eq.(6). Near the polarity reversal boundary $C_{\rm bg}V_{\rm bg} + C_{\rm tg}V_{\rm tg} = 0$ (white dashed line in Fig.1a), using the device parameters $C_{\rm bg} = 115\,{\rm aF}/\mu{\rm m}^2$, $V_{\rm bg} = -70\,{\rm V}$, $w = 50\,{\rm nm}$, we find $B_c = (\hbar/ew)\left(\pi C_{\rm bg}V_{\rm bg}/e\right)^{1/2} \approx 5.2\,{\rm T}$.

The dependence of B_c on experimental control parameters $V_{\rm tg}$ and $V_{\rm bg}$ can be obtained by analyzing the turning points for the density profile (5). Setting $p_y = 0$ gives $\hbar k_F(x) = \pm eBx$. Solving this equation and equating the result to barrier half-width, $x_{1(2)} = \pm w$, we obtain

$$B_c = (\hbar/ew)\sqrt{(2\pi/eg)(2C_{\rm bg}V_{\rm bg} + C_{\rm tg}V_{\rm tg})}. \quad (7)$$

Both the value of B_c and its dependence on gate voltages matches the data quite well (red line in Fig.1b).

The actual density profile is nonparabolic, flattening outside the top gate region (TGR) on a length scale $2w \approx 100\,{\rm nm}$. Yet, since the magnetic length ℓ_B is much shorter than $2w$ for the fields of interest ($B \gtrsim 1\,{\rm T}$), this flattening does not significantly impact our discussion of the collapse phenomenon. While the states realized at subcritical magnetic fields are not truly deconfined due to cyclotron motion in the region outside the TGR, the corresponding orbits are very long. For such states, the particle traverses the TGR, makes a partial cyclotron orbit outside of the TGR, and finally crosses the TGR again to close the orbit (Fig.3a). The net orbit length is a few w, which is much greater than the orbit size at strong fields (a few ℓ_B). The contribution of long orbits to SdH oscillations will be suppressed due to spatial inhomogeneity and disorder scattering; hence the distinction between confined and deconfined orbits remains sharp despite the flattening of the potential (also, see a more detailed discussion in Online Supplement [19]).

With that in mind, below we analyze a simple model, $U(x) = -ax^2$. A simple estimate of the collapse threshold can be obtained by considering balance between the Lorentz force and the force due to the electric field, $v_F B = -dU/dx$. This condition is satisfied for a particle moving parallel to the barrier with $x = \pm\ell$, $\ell = ev_F B/(2a)$. This gives an energy-dependent critical field,

$$B_c(\varepsilon) = (2/ev_F)\sqrt{-a\varepsilon}, \quad (8)$$

which increases with detuning from neutrality, as in experiment.

We treat the problem using microscopic Hamiltonian

$$H = \begin{pmatrix} U(x) & v_F p_- \\ v_F p_+ & U(x) \end{pmatrix}, \quad p_\pm = -i\hbar\frac{d}{dx} \pm i(p_y - eBx), \quad (9)$$

where p_y is the conserved canonical momentum component parallel to the barrier. We nondimensionalize the problem using "natural units"

$$\varepsilon_* = (\hbar^2 v_F^2 a)^{1/3}, \;\; x_* = \left(\frac{v_F\hbar}{a}\right)^{1/3}, \;\; B_* = \frac{\hbar}{e}\left(\frac{a}{v_F\hbar}\right)^{2/3}.$$

For each value of p_y and magnetic field B, we represent the Hamiltonian as an $M \times M$ matrix defined on a grid in position space, with periodic boundary conditions. We use the eigenvalues and eigenstates obtained from diagonalization to evaluate the local density of states (DOS) in the middle of the barrier,

$$N(\varepsilon) = \int \frac{dp_y}{2\pi}\sum_{n=1}^{M}\frac{\Gamma}{\pi}\frac{\langle|\psi_{n,p_y}(x=0)|^2\rangle}{(\varepsilon-\varepsilon_n)^2+\Gamma^2}, \quad (10)$$

with Landau level broadening incorporated through the Lorentzian width $\Gamma = 0.2\varepsilon_*$. In our simulation, a system of size $L = 15x_*$ discretized with $M = 1500$ points was used. Averaging with a gaussian weight was used to suppress the effect of spurious states arising due to a vector potential jump at the boundary,

$$\langle|\psi_{n,p_y}(x=0)|^2\rangle = \int dx' e^{-x'^2/2\sigma^2}|\psi_{n,p_y}(x')|^2, \quad (11)$$

with $\sigma \approx x_*$. Oscillations in the density of states (10) modulate the rate of electron scattering by disorder, and thus show up in transport quantities measured as a function of experimental control parameters, as in the canonical SdH effect [18].

The resulting local DOS exhibits oscillations which track Landau levels at high B (Fig.1d). In the pp′p case, at lower B, discrete Landau levels give way to a continuous spectrum in the region inside a parabola (dashed line) which marks the collapse threshold, Eq.(8).

The DOS exhibits FP fringes in the pnp region at low B, however without the the half-period shift seen in $dG/dV_{\rm tg}$ at $B \lesssim 1T$ (Fig.1). As discussed in Ref.[14], this half-period shift results from FP interference due to Klein scattering at pn interfaces. A proper model of this effect must account for ballistic transport in the system.

The collapse observed in the density of states is related to deconfinement of classical orbits. The orbits can be analyzed as constant energy trajectories of the problem

$$\varepsilon = v_F\sqrt{p_x^2 + \tilde{p}_y^2} + U(x), \quad \tilde{p}_y = p_y - eBx. \quad (12)$$

For parabolic $U(x) = -ax^2$ the orbits with $p_y = 0$ can be easily found in polar coordinates $p_x + ip_y = |p|e^{i\theta}$:

$$\frac{|p|}{p_0} = \frac{1}{\sin^2\theta}\left(1 \pm \sqrt{1 - \frac{\varepsilon}{\varepsilon_c}\sin^2\theta}\right), \quad \varepsilon_c = \frac{(v_F eB)^2}{4a} \quad (13)$$

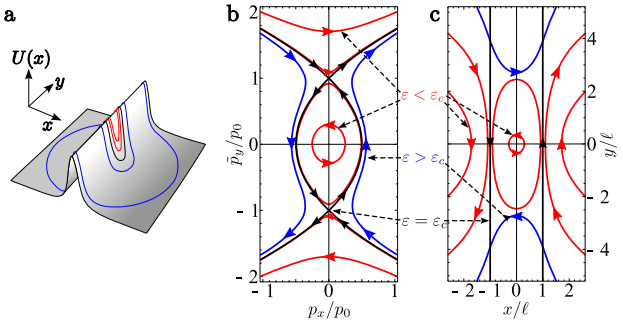

FIG. 3: (a) Closed orbits for the Thomas-Fermi potential obtained from the density profile, Eq.(5), with $B = 9, 7, 5, 3, 1$ T and $p_y = 0$. Long trajectories, extending far outside the gated region, do not contribute to SdH oscillations (see text). (b,c) Trajectories for the potential $U(x) = -ax^2$ and $p_y = 0$. Three types of trajectories are shown in momentum space (b) and position space (c): subcritical (red), critical (black), and supercritical (blue). The saddle points in momentum space correspond to motion along straight lines $x = \pm\ell$, where the Lorentz force is balanced by the electric field.

with $p_0 = v_F e^2 B^2/2a$ (see Fig.3b). Only real, positive solutions should be retained; when $\varepsilon/\varepsilon_c > 1$, the discriminant in Eq.(13) is negative near $\theta \approx \pi/2$ and trajectories cannot close (blue curves in Fig.3b).

The related orbits in position space can be found from the relation $dy/dx = \dot{y}/\dot{x} = \tilde{p}_y/p_x$, giving

$$\frac{dy}{dx} = \frac{\pm v_F(p_y - eBx)}{\sqrt{(\varepsilon - U(x))^2 - v_F^2(p_y - eBx)^2}}. \qquad (14)$$

For $p_y = 0$, integration is performed using the variable $u = x^2/\ell^2$,

$$\frac{y}{\ell} = \pm \int \frac{du}{\sqrt{(u + \varepsilon/\varepsilon_c - 2)^2 + 4(\varepsilon/\varepsilon_c - 1)}}, \qquad (15)$$

where $\ell = v_F eB/2a$ such that $\varepsilon_c = a\ell^2$. The integrand changes its behavior at the critical energy ε_c. For $\varepsilon > \varepsilon_c$, the integrand is real valued for all u and

$$\sinh\left(\frac{y(x) - y_0}{\ell}\right) = \frac{x^2/\ell^2 + \varepsilon/\varepsilon_c - 2}{2\sqrt{\varepsilon/\varepsilon_c - 1}}. \qquad (16)$$

For $\varepsilon < \varepsilon_c$, real solutions are divided into two domains $0 \le u \le 2 - \varepsilon/\varepsilon_c - 2\sqrt{1 - \varepsilon/\varepsilon_c}$ (closed orbits) and $u > 2 - \varepsilon/\varepsilon_c + 2\sqrt{1 - \varepsilon/\varepsilon_c}$ (open orbits):

$$\cosh\left(\frac{y(x) - y_0}{\ell}\right) = \pm\frac{2 - \varepsilon/\varepsilon_c - x^2/\ell^2}{2\sqrt{1 - \varepsilon/\varepsilon_c}}. \qquad (17)$$

The red curves in Fig.3c correspond to the low energy regime, $\varepsilon < \varepsilon_c$, where orbits can either be closed (Landau levels) or open (trajectories for particle moving far from the barrier). At higher energies, $\varepsilon > \varepsilon_c$, all trajectories are open. The straight black lines correspond to the critical orbits of Eq.(8), where the Lorentz force and electric field are balanced. In addition to the two particular critical trajectories shown, in the limit $\varepsilon/\varepsilon_c \to 1$ there is an entire family of critical trajectories which asymptotically approach these lines.

Interestingly, unlike in the case of the potential obtained from the Thomas-Fermi model, where the classical turning points move continuously to infinity as the transition is approached, trajectories in the parabolic potential are trapped between the critical separatrix lines. At very low energies, closed orbits are approximately circular; as the energy increases towards ε_c, orbits become more and more elongated, until finally merging with the separatrix at $\varepsilon = \varepsilon_c$ (see Fig.3).

In summary, graphene devices with a barrier induced by a narrow top gate can be used to probe electronic states on the spatial scale of a few tens of nanometers. In our transport measurements, the SdH-type resonances arising from quantized states associated with closed orbits are used to directly observe the competition between magnetic confinement and deconfinement due to electric field. As a result of this competition, the discrete spectrum of Landau levels collapses when subjected to a strong external potential. Experimental observations are found to be in good agreement with theory.

MSR acknowledges NSF support under DMR090647 and PHY0646094. PK acknowledges support from NRI, INDEX, ONR MURI, and FENA. LSL acknowledges ONR support under N00014-09-1-0724.

[1] M. S. Khaikin, Adv. Phys. 18, 1 (1969).
[2] V. S. Tsoi, J. Bass, P. Wyder, Rev. Mod. Phys. 71, 1641 (1999).
[3] M. L. Roukes *et al.*, Phys. Rev. Lett. **59**, 3011 (1987).
[4] C. J. B. Ford *et al.*, Phys. Rev. Lett. **62**, 2724 (1989).
[5] D. Weiss *et al.*, Europhys. Lett. **8**, 179 (1989);
[6] D. Weiss *et al.*, Phys. Rev. Lett. 66, 2790 (1991)
[7] H. van Houten *et al.*, Phys. Rev. B 39, 8556 (1989)
[8] K. S. Novoselov *et al.*, Science, **306**, 666 (2004)
[9] J. P. Lu, X Ying, and M. Shayegan. Appl. Phys. Lett. **65**, 2320(1994).
[10] B. Huard *et al.*, Phys. Rev. Lett. 98, 236803 (2007).
[11] J. R. Williams, L. DiCarlo, C. M. Marcus, Science 317, 638 (2007).
[12] B. Özyilmaz *et al.*, Phys. Rev. Lett. 99, 166804 (2007).
[13] A. F. Young, P. Kim, Nature Phys. **5**, 222 (2009).
[14] A. V. Shytov, M. S. Rudner, L. S. Levitov, Phys. Rev. Lett. 101, 156804 (2008)
[15] V. Lukose, R. Shankar, G. Baskaran, Phys. Rev. Lett. **98**, 116802 (2007).
[16] A. Shytov *et al.*, Solid State Comm. **149**, 1087 (2009).
[17] L. M. Zhang, M. M. Fogler, Phys. Rev. Lett. **100**, 116804 (2008).
[18] A. A. Abrikosov, *Introduction to the theory of normal metals* (Academic Press, New York, 1972).
[19] Supplementary Online Material